Biosensors and Bioelectronics 129 (2019) 118–123

Contents lists available at ScienceDirect

Biosensors and Bioelectronics

journal homepage: www.elsevier.com/locate/bios

A ratiometric nanoprobe for biosensing based on green fluorescent graphitic carbon nitride nanosheets as an internal reference and quenching platform

Xueting Liu[a], Huijun Zhang[a], Zhiping Song[a], Liangqia Guo[a,*], Fengfu Fu[a], Yongning Wu[b]

[a] Ministry of Education Key Laboratory of Analytical Science of Food Safety and Biology, Fujian Provincial Key Laboratory of Analysis and Detection Technology for Food Safety, College of Chemistry, Fuzhou University, Fuzhou 350116, China
[b] China National Center for Food Safety Risk Assessment, Beijing 100022, China

ARTICLE INFO

Keywords:
g-C_3N_4
Ratiometric nanoprobe
Fluorescent quenching
Internal reference
Aptamer

ABSTRACT

The integrating of high fluorescent quenching capability of two-dimensional nanomaterials with dye-labelled ssDNA as nanoprobes has attracted increasing interest for biosensing applications. However, this absolute intensity-dependent single fluorescent signal may be influenced by target concentration-independent factors. To overcome this challenge, a ratiometric nanoprobe was developed by utilizing green fluorescent phenyl-doped carbon nitride (PDCN) nanosheets as an internal reference and quenching platform. 5-carboxy-X-rhodamine-labelled anti-adenosine aptamer was used as a signal probe. PDCN nanosheets quenched the fluorescence of the absorbed signal probe while kept their own fluorescence constantly. Upon addition of adenosine, the formation of adenosine-aptamer complexes led to desorption of the signal probe from the surface of PDCN nanosheets, resulted in the fluorescent recovery of the signal probe. The ratio of the fluorescent enhancement of the signal probe to the inherent fluorescence of PDCN nanosheets was used to quantitatively measure adenosine. The limit of detection for adenosine was 6.86 μM. Finally, the ratiometric nanoprobe was applied to determine adenosine in serum samples.

1. Introduction

With the increasing demand for disease diagnosis and therapies, fluorescent biosensors become powerful tools to monitor biological analytes, such as metal ions, nucleic acid, protein, and small biomolecules (Hu et al., 2017). Generally, the molecular recognition element and the signal transduction element are two important components in biosensors (Liu et al., 2015). Functional single-stranded DNA (ssDNA) probes are often used as molecular recognition elements due to their high chemical stability, excellent recognition ability, cost-effective synthesis, easy modification (Liu et al., 2009). Two-dimensional (2D) nanomaterials have emerged as promising nanoquenchers in fluorescent biosensors due to their unique properties such as large specific surface area, good biocompatibility, highly fluorescent quenching capabilities (Zhu et al., 2015; Anichini et al., 2018). Furthermore, 2D nanomaterials usually exhibit much stronger interactions with ssDNA than double-stranded DNA (dsDNA) (Mo et al., 2017). Hence, dye-labelled ssDNA probes/aptamers can be absorbed on the surface of 2D nanomaterials, resulting in the fluorescent quenching based on the mechanism such as fluorescence resonance energy transfer (FRET), photo-induced electron transfer (PET) and so on (Tian et al., 2017). While in the presence of complementary ssDNA strands or target molecules to hybrid with the ssDNA probes or to change the configuration of aptamers, the resulting dsDNA duplexes or aptamer-target complexes desorb from the surface of 2D nanomaterials and the dye's fluorescence is recovered. Graphene and graphene oxide are the typical 2D nanomaterial for biosensing through the assembly of ssDNA probes onto their surface via π-π stacking and hydrophobic interactions between nucleobases and basal plane of graphene (Lu et al., 2009; Loh et al., 2010; Wang et al., 2010; Y. Wang et al., 2013; Wang et al., 2014; Wang et al., 2017). Graphene-like layered nanomaterials such as graphdiyne (Wang et al., 2016), graphitic carbon nitride (g-C_3N_4) (G.B. Wang et al., 2013; Liao et al., 2014), transition metal dichalcogenides (TMDCs) (e.g., MoS_2, WS_2, WSe_2, TiS_2, TaS_2) (Zhu et al., 2013; Xi et al., 2014; Song et al., 2018; Sun et al., 2017; Zhang et al., 2015), ternary chalcogenides (e.g., Ta_2NiS_5, Ta_2NiSe_5) (Tan et al., 2015), transition metal oxides (e.g., MnO_2) (Yuan et al., 2017; Cai et al., 2015) exhibit similar physisorption and fluorescent quenching abilities, and have also been applied in fluorescent biosensing system. Although great progresses have been made in 2D nanomaterials-based fluorescent biosensors, target concentration based on the absolute intensity acquisition from a single signal may be influenced by the change of the probe

* Corresponding author.
E-mail address: lqguo@fzu.edu.cn (L. Guo).

https://doi.org/10.1016/j.bios.2019.01.032
Received 12 October 2018; Received in revised form 21 December 2018; Accepted 7 January 2019
Available online 22 January 2019
0956-5663/

concentration, instrumentation variables such as fluctuation of the light source or detector, or environmental factors in complex samples (Huang et al., 2018; Chen et al., 2018)

Encouragingly, besides the strong affinity toward ssDNA via π-π interactions and fluorescent quenching ability toward fluorescent dyes via PET (G.B. Wang et al., 2013; Liao et al., 2014), g-C_3N_4 nanomaterials also possess excellent fluorescent property originating from the high-degree condensation of the tri-s-triazine units (Yang et al., 2015). g-C_3N_4 nanosheets or quantum dots, which are prepared by exfoliating from their bulk through mechanical or chemical methods, exhibit high quantum yields and stability, good biocompatibility, low toxicity, making them great potential applications in biosensing and bioimaging (Tang et al., 2013; Zhang et al., 2013; X.L. Zhang et al., 2014; X.D. Zhang et al., 2014; Liu et al., 2016). Unfortunately, due to the large bandgap (~ 2.7 eV) most g-C_3N_4 nanomaterials emit near ultraviolet-blue fluorescence (Song et al., 2016), which is apt to interfere by biological self-fluorescence (Wu et al., 2016). Recently, Jingsan Xu's group (Cui et al., 2016) and our group (Song et al., 2017) developed different methods to synthesize phenyl-doped g-C_3N_4 (PDCN) nanomaterials with strong green fluorescence, which render them more apposite candidates for fluorescent biosensing. Herein we develop a ratiometric nanoprobe by utilizing PDCN nanosheets as an internal reference and quenching platform. As shown in Scheme 1, a dye-labelled aptamer is adsorbed on the surface of PDCN nanosheets and its fluorescence is quenched, while the fluorescence of PDCN nanosheets is almost unchanged. Upon addition of the target, the formation of the target-aptamer complexes results in the recovery of dye's fluorescence. The target concentration-dependent fluorescent signal can be normalized by the inherent fluorescence of PDCN nanosheets. Thus, a ratiometric fluorescent biosensor is achieved, which can facilitate more accurate and reliable quantitation of the target (Huang et al., 2018). Adenosine plays an important role in multiple physiological activities and is also considered as a possible biomarker for cancer. Sensitive, accurate and reliable detection of adenosine is of great significance for clinical disease diagnosis and treatment (Hashemian et al., 2016; Shi et al., 2018). Although the aptasensors based on time-resolution luminescence (Li et al., 2012), electrochemistry (Yan et al., 2011), Raman (Xu et al., 2015) and the fluorescence quenching of other nanomaterials (He et al., 2010; Luo et al., 2012; Fu et al., 2013; Zhu et al., 2013) have been reported for the detection of adenosine, the ratiometric fluorescent aptasensor for adenosine has not been reported yet. Therefore, adenosine is chosen as a model target to verify the 2D nanomaterials-based ratiometric biosensing strategy.

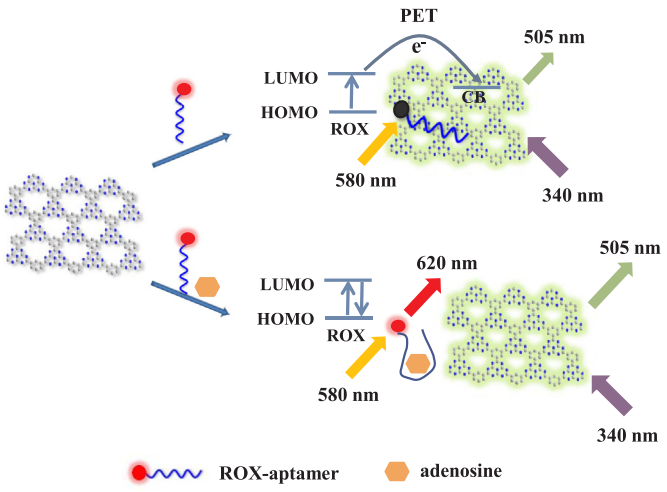

Scheme 1. The ratiometric biosensing strategy for adenosine by using PDCN nanosheets as an internal reference and quenching platform.

2. Experimental section

2.1. Reagents and materials

HPLC-purified carboxy-X-rhodamine (ROX)-labelled anti-adenosine aptamer (5′-ROX-AAC CTG GGG GAG TAT TGC GGA GGA AGGT-3′, ROX-aptamer), adenosine, guanosine, cytimidine, uridine, thymidine and ascorbic acid were purchased from Shanghai Sangon biological engineering technology and service Co., Ltd. Cysteine, glycine and phenylalanine were purchased from Shanghai Kangda amino acid factory. Human serum albumin (HSA) was purchased from Shanghai Yuanye Bio-Technology Co., Ltd. Urea, trimesic acid and all other chemicals were analytical grade and purchased from Sigma-Aldrich. Tris-HCl buffer (20 mM, pH 7.4, 100 mM NaCl, 5 mM KCl, 5 mM $MgCl_2$) was used as the buffer solution for biosensing. Ultrapure water (18.2 MΩ cm) was purified by a Millipore system and used throughout the experiment.

2.2. Characterization

Transmission electron microscopy (TEM) images were obtained by an FEI Tecnai G2F20 transmission electron microscope. Before measurement, the dispersion solution of PDCN nanosheets was deposited on a carbon film supported by copper grids. X-ray photoelectron spectroscopy (XPS) data were collected by a Thermo Scientific ESCALAB 250 with an Al Kα source (1486.6 eV). X-ray diffraction (XRD) patterns were characterized by a Bruker D8 advance diffractometer with Cu Kα1 radiation (λ = 1.5406 Å). Fourier transform infrared (FT-IR) spectra were recorded on a Nicolet 6700 FT-IR spectrometer using a KBr pellet, scanning from 4000 to 400 cm^{-1} at room temperature. Dynamic light scattering data (DLS) were corrected by a Malvern Zetasizer Nano-2s laser particle size and zeta potential analyzer. An atomic force microscopy (AFM) image was obtained on a Bruker Nanoscope IIID scanning probe microscopy system. Fluorescence spectra were measured by a Hitachi F4600 spectrofluorometer.

2.3. Preparation of PDCN nanosheets

PDCN powder was prepared according to our previous work (Song et al., 2017). Specially, 10 g urea and 0.01 g trimesic acid were dissolved in 15 mL distilled water and the solution was evaporated to dry. Then, the mixture was placed in an alumina crucible with a cover and heated to 500 °C for 2 h at a heating rate of 5 °C min^{-1} under nitrogen gas phenomenon. After cooling to room temperature, the yellow powder was ultrasonicated in water for 10 h. The mixture solution was centrifuged at 5000 rpm for 5 min twice to remove the unexfoliated particles. The concentration of PDCN nanosheets dispersion was determined to be 0.4 mg mL^{-1}.

2.4. Ratiometric biosensing for adenosine

12 μL ROX-aptamer (1 μM) and adenosine with different concentration were incubated in 308 μL Tris-HCl buffer (20 mM, pH 7.4) for 30 min. Then, 80 μL PDCN nanosheets (0.4 mg mL^{-1}) was added and the mixture was further incubated at 37 °C for 10 min. The fluorescent spectra of the mixture was measured by the excitation wavelength at 580 nm with emission scan range from 590 nm to 800 nm for ROX, while the excitation wavelength at 340 nm with emission scan range from 360 nm to 600 nm for PDCN nanosheets.

3. Results and discussion

3.1. Characterization of PDCN nanosheets

The morphology of PDCN nanosheets was characterized by AFM (Fig. 1AB) and TEM images (Fig. S1). The thickness of PDCN nanosheets

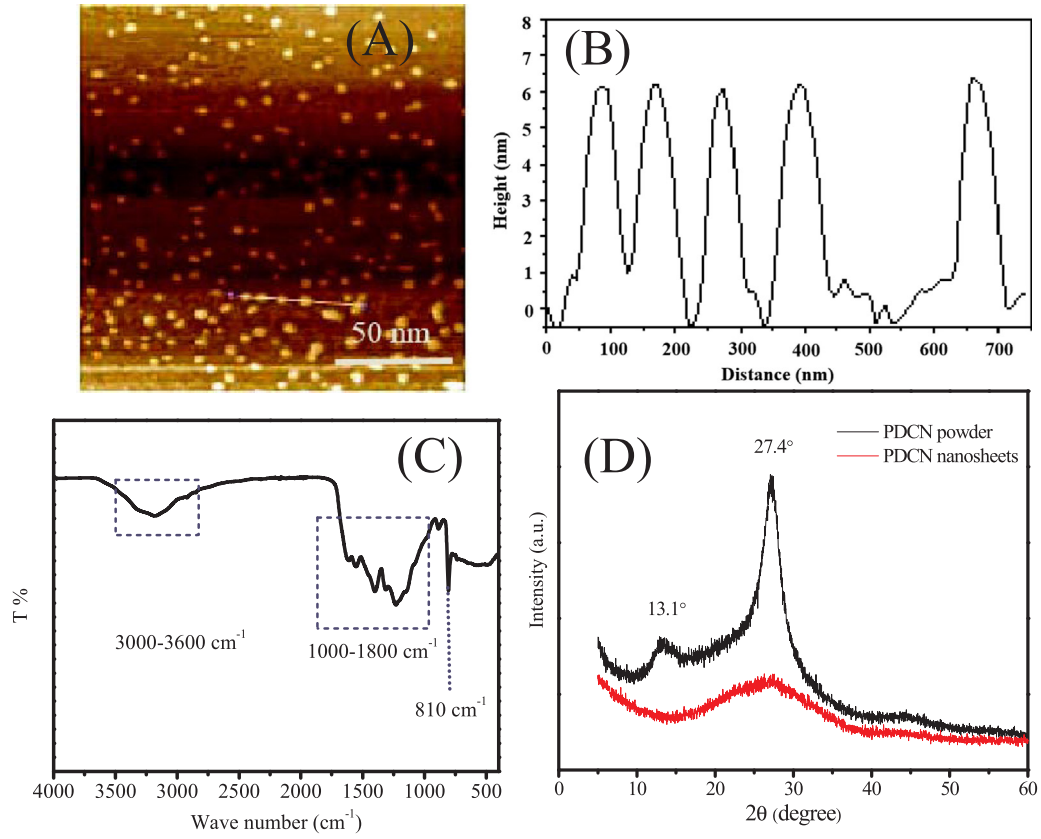

Fig. 1. AFM image (A), height profile (B), FT-IR spectrum (C) of PDCN nanosheets and XRD patterns (D) of PDCN powder and PDCN nanosheets.

is about 6 nm and the size is about 130 nm. From the DLS data (Fig. S2), the most probable dynamic diameter and the zeta potential of PDCN nanosheets were about 150 nm and −35 mV, respectively, indicating the good stability and dispersion of PDCN nanosheets. The chemical composition of PDCN nanosheets was investigated by XPS and FT-IR spectra. As shown in Fig. S3A, besides the O1s peak due to the surface absorbed H_2O (Song et al., 2017). PDCN nanosheets show two main peaks of carbon and nitrogen elements. The C1s XPS spectrum (Fig. S3B) can be deconvoluted into two peaks with the binding energies of 287.8 eV and 284.6 eV. The peak of 287.8 eV can be assigned to the sp2-bonded carbon (C–C=N). Another peak of 284.6 eV is ascribed to standard reference carbon (C–C) (Zhang et al., 2013). The N 1s core-level spectrum (Fig. S3C) can be deconvoluted into three peaks with the binding energies at 398.1, 399.2 and 400.6 eV. The strongest N 1s peak at 398.1 eV is assigned to the sp2-bonded nitrogen in N-containing aromatic rings (CN=C), whereas the weak peak at 399.2 eV is usually attributed to the tertiary nitrogen $N(C)_3$ groups. The peak at 400.6 eV indicates the presence of amino groups (C-N-H) (Lin and Wang, 2013). FT-IR spectrum (Fig. 1C) of PDCN nanosheets features the characteristic vibration peak of triazine units at 810 cm^{-1}, typical stretching modes of aromatic heterocycles of g-C_3N_4 at 1200–1600 cm^{-1}, and stretching modes of -NH_2 and -OH groups at 3000–3600 cm^{-1} (Lin and Wang, 2013). As shown in Fig. 1D, the strong XRD peak at 27.4° in bulk PDCN is originated from the interlayer diffraction of graphitic-like structures, corresponding to an interlayer distance of d = 0.326 nm. Noticeably, the intensity of this peak for PDCN nanosheets is sharply decreased, suggesting the few-layered structure after successful exfoliation. The low angle diffraction peak at 13.3° (d = 0.663 nm), which is derived from the in-planar repeated tri-s-triazine units, becomes less pronounced for the nanosheets because of the simultaneously decreased planar size of the carbon nitride layers after exfoliation (Ma et al., 2014).

3.2. Fluorescent quenching property and mechanism of PDCN nanosheets

After addition of ROX-aptamer into the dispersion solution of PDCN nanosheets, ROX-aptamer was adsorbed on the surface of PDCN nanosheets via π-π stacking and hydrophobic interactions between nucleobases and basal plane of PDCN nanosheets; The most probable dynamic diameter of PDCN nanosheets was increased to 180 nm and the zeta potential was decreased to −40 mV (Fig. S2) due to the absorption of ROX-aptamer on the surface of PDCN nanosheets, resulting in the better stability and dispersion. As shown in Fig. 2A, the dispersion solution of PDCN nanosheets emits strong green fluorescence with the maximal excitation and emission wavelengths at 320 nm and 505 nm, respectively. When the excitation wavelength is larger than 400 nm, PDCN nanosheets do not fluoresce. Next, the fluorescent quenching ability of PDCN nanosheets was investigated by mixing 30 nM ROX-aptamer with different concentration of PDCN nanosheets. 90% of ROX fluorescence is quenched with 10 min after addition of PDCN nanosheets (Fig. S4). As shown in Fig. 2B, the fluorescent intensity of ROX under the excitation of 580 nm was decreased as the concentration of PDCN nanosheets was increased, which indicated PDCN nanosheets also possessed strong fluorescent quenching ability toward ROX. When the concentration of PDCN nanosheets reached 0.1 mg mL^{-1}, the fluorescence of ROX was almost completely quenched by PDCN nanosheets. However, under the excitation of 340 nm, the fluorescence of PDCN nanosheets was almost not decreased and there was almost no emission of ROX (Fig. S5). So, there was no FRET between PDCN nanosheets and ROX-aptamer. If FRET was present, the efficiency would be very low. As shown in Scheme 1, the fluorescence quenching of ROX-aptamer was mainly due to the transfer of the photoexcited electrons from the lowest unoccupied molecular orbital (LUMO) of ROX to the conductive band (CB) of PDCN nanosheets (G.B. Wang et al., 2013; Liao et al., 2014). In the presence of adenosine, the formation of aptamer-adenosine complex might induce ROX-aptamer to

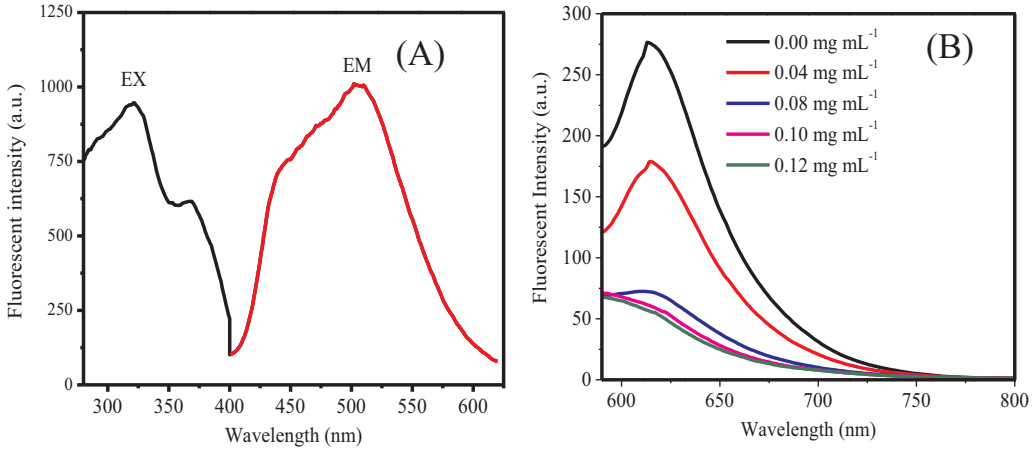

Fig. 2. Fluorescent spectra of PDCN nanosheets dispersion (A) and fluorescent spectra of 30 nM ROX-aptamer mixed with different concentrations of PDCN nanosheets when excited at 580 nm (B).

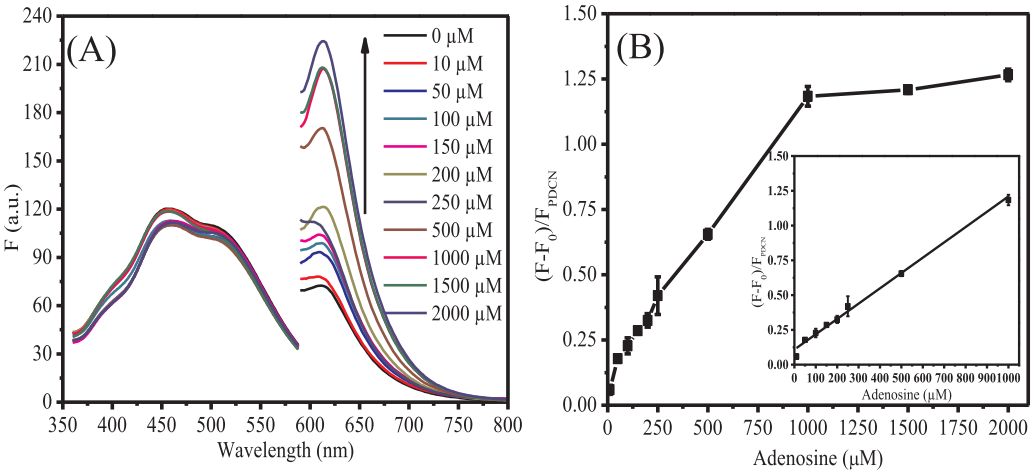

Fig. 3. (A) Fluorescent emission spectra of PDCN nanosheets (λ_{EX} = 340 nm) and ROX-aptamer (λ_{EX} = 580 nm) after addition of different concentrations of adenosine; (B) The ratio value of fluorescent intensity ($(F-F_0)/F_{PDCN}$) as a function of adenosine concentration. Insert of B was the calibration curve for adenosine.

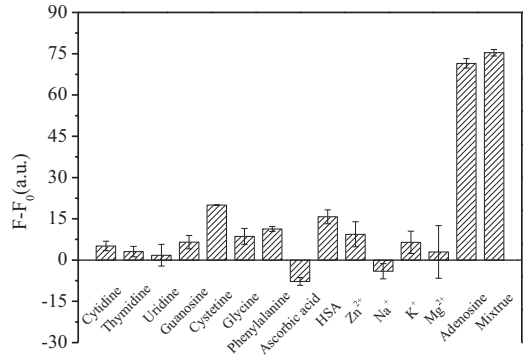

Fig. 4. Fluorescent enhancement of the biosensor in the presence of 500 μM adenosine, 1 mM guanosine, 1 mM cytimidine, 1 mM thymine, 1 mM uridine, 1 mM cysteine, 1 mM glycine, 1 mM phenylalanine, 1 mM ascorbic acid, 1 mM Zn^{2+}, 1 mM Na^+, 1 mM K^+, 1 mM Mg^{2+}, 50 mg mL^{-1} HSA and the mixture of 1 mM guanosine, 1 mM cytimidine, 1 mM thymine, 1 mM uridine and 500 μM adenosine.

desorb from the surface of PDCN nanosheets, resulting in the fluorescence recovery due to the removal of PET process. Therefore, the ratiometric method can be developed by normalizing the fluorescence intensity of ROX-aptamer by the fluorescence intensity of PDCN nanosheets. Therefore, it is possible to design a ratiometric nanoprobe for biosensing of adenosine by taking advantage of PDCN nanosheets as an internal reference and quenching platform.

3.3. Optimal biosensing conditions

In order to achieve the best performance of the nanoprobe, the reaction conditions such as the concentration of PDCN nanosheets, incubation time, buffer pH were optimized by measuring the fluorescent enhancement ($F-F_0$) of the signal probe after addition of adenosine, where F_0 and F represented the fluorescent intensity of ROX-aptamer at 620 nm in the absence and presence of adenosine, respectively. For simplicity, only the fluorescent signal of ROX-aptamer was measured. As shown in Fig. S6A, the fluorescent enhancement reaches the maximum at 0.08 mg mL^{-1} PDCN nanosheets. The fluorescent enhancement is increasing with the incubation time for the formation of adenosine-aptamer complexes. As shown in Fig. S6B, when the incubation time is longer than 30 min, the fluorescent enhancement reached the plateau. The fluorescent enhancement is increased with the increasing pH of Tri-HCl buffer but decreased when the pH value is higher than 7.4 (Fig. S6C). Therefore, 0.08 mg mL^{-1} PDCN nanosheets, 30 min incubation time and pH 7.4 of Tris-HCl buffer were chosen for further experiments. In addition, the photostability of the nanoprobe was also investigated (Fig. S7); the fluorescence intensities of PDCN nanosheets and ROX-aptamer almost did not change within continuous excitation for 30 min, indicating the excellent photostability of the nanoprobe.

Table 1
Measurement of spiked adenosine in serum samples by this biosensor.

Samples	Original (μM)	Added (μM)	Found (μM, n = 5) mean ± SD	Recovery (%)	RSD (%)
1	67	100	164 ± 7	97	4.6
2	67	500	570 ± 20	101	3.5
3	67	750	824 ± 32	101	3.9

3.4. Ratiometric biosensing of adenosine

The ratiometric nanoprobe for biosensing of adenosine was explored under the excitation wavelengths of 340 nm and 580 nm. Fig. 3A showed the fluorescent spectra of the biosensor on addition of different concentrations of adenosine. With the increasing concentrations of adenosine from 0 to 2000 μM the fluorescence of ROX-aptamer is gradually recovered while the fluorescence of PDCN nanosheets is almost constant. The ratio of the fluorescent enhancement ($F-F_0$) of ROX-aptamer at 620 nm to the fluorescent intensity of PDCN nanosheets at 505 nm (F_{PDCN}) is increased with the increasing concentration of adenosine (Fig. 3B). The linear range for the detection of adenosine is 10–1000 μM (R^2 = 0.9935). The limit of detection is 6.86 μM according to the 3σ rule. A comparison with other published aptasensors for adenosine (Table S1), the sensitivity of this method was comparable to the time-resolved luminescence method (Li et al., 2012), HCR-based fluorescence method (Fu et al., 2013), MoS_2-based fluorescence (Zhu et al., 2013), GO-based fluorescence method (He et al., 2010). And this method also showed a wide linear response range for the detection of adenosine. The linear range based on the single fluorescence signal of ROX-aptamer was also constructed (Fig. S8) and covered the range of 50–500 μM (R^2 = 0.9888). This result indicated the ratiometric fluorescence sensor with PDCN nanosheets as the internal reference could eliminate some concentration-independence errors and broadened the linear range.

To challenge the anti-interference ability of this biosensor, the fluorescent enhancements of the signal probe on addition of the analogues of adenosine, amino acids (such as cysteine, glycine, phenylalanine), ascorbic acid, metal ions (such as Zn^{2+}, Na^+, K^+, Mg^{2+}), HSA and the mixture of adenosine with its analogues were measured, respectively. As shown in Fig. 4, although the concentrations of these possible interferents are higher than that of adenosine, the fluorescent enhancement of these analogues is much lower than that of adenosine. Furthermore, the mixture of these analogues also do not interfere the detection of adenosine. Therefore, this biosensor exhibits good selectivity for adenosine.

To demonstrate the potential application of this biosensor for adenosine, human serum samples were 100-fold diluted with Tris-HCl buffer (20 mM, pH 7.4) and the protein was removed by centrifugation at 8000 rpm for 10 min. Different concentrations of adenosine were spiked and measured by this biosensor. The results were listed in Table 1. The recoveries are ranged from 97% to 101% and the RSD are less than 5%, which indicate this biosensor may be potentially applied for the detection of adenosine in human serum.

4. Conclusion

In this work, green fluorescent PDCN nanosheets were prepared by copolymerization urea with a small amount of trimesic acid, followed by ultrasonic exfoliation in water. After the signal probe ROX-labelled anti-adenosine aptamer is adsorbed on the surface of PDCN nanosheets, the fluorescence of the signal probe is quenched via the PET mechanism while the fluorescence of PDCN nanosheets is almost unchanged. On addition of adenosine, the formation of adenosine-aptamer complexes results in desorption of the signal probe from the surface of PDCN nanosheets and fluorescent recovery of the signal probe. Therefore, a ratiometric biosensor for adenosine in human serum was developed with acceptable sensitivity, reproducibility and selectivity by the ratio of fluorescent enhancement of the signal probe to the fluorescence of PDCN nanosheets. The introduction of green fluorescent PDCN nanosheets as the internal reference can greatly reduce the influence of target concentration-independent factors in biosensing applications. Although two emission scans need to be taken due to the different excitation wavelength of PDCN nanosheets and ROX-aptamer, we believe this ratiometric strategy will expand the general scope of 2D nanomaterials-based biosensing applications.

Acknowledgements

The authors are thankful for the support from the National Natural Science Foundation of China (21874023, 21577017), the National Key Research and Development Program of China (2017YFC1600500) and the Program for Chang jiang Scholars and Innovative Research Team in University of Ministry of Education of China (IRT15R11).

Declaration of interests

None.

Appendix A. Supporting information

Supplementary data associated with this article can be found in the online version at doi.org/10.1016/j.bios.2019.01.032.

References

Anichini, C., Czepa, W., Pakulski, D., Aliprandi, A., Ciesielski, A., Samori, P., 2018. Chem. Soc. Rev. 47, 4860–4908.
Cai, Q.Y., Li, J., Ge, J., Zhang, L., Hu, Y.L., Li, Z.H., Qu, L.B., 2015. Biosens. Bioelectron. 72, 31–36.
Chen, L., Song, Z.P., Liu, X.T., Guo, L.Q., Li, M.J., Fu, F.F., 2018. Analyst 143, 1609–1614.
Cui, Q.L., Xu, J.S., Wang, X.Y., Li, L.D., Antonietti, M., Shalom, M., 2016. Angew. Chem. Int. Ed. 55, 3672–3676.
Fu, B., Cao, J., Jiang, W., 2013. Biosens. Bioelectron. 44, 52–56.
Hashemian, T., Saraji, M., Shirani, M.P., 2016. Biosens. Bioelectron. 79, 334–340.
He, S.J., Song, B., Li, D., Zhu, C.F., Qi, W.P., Wen, Y.Q., Wang, L.H., Song, Z.P., Fang, H.P., Fan, C.H., 2010. Adv. Funct. Mater. 20, 453–459.
Hu, Y.L., Huang, Y., Tan, C.L., Zhang, X., Lu, Q.P., 2017. Mater. Chem. Front. 1, 24–36.
Huang, X.L., Song, J.B., Yung, B.C., Huang, X.H., Xiong, Y.H., Chen, X.Y., 2018. Chem. Soc. Rev. 47, 2873–2920.
Li, L.L., Ge, P., Selvin, P.R., Lu, Y., 2012. Anal. Chem. 84, 7852–7856.
Liao, X., Wang, Q., Ju, H., 2014. Chem. Commun. 50, 13604–13607.
Lin, Z.Z., Wang, X.C., 2013. Angew. Chem. Int. Ed. 52, 1735–1738.
Liu, J.W., Cao, Z.H., Lu, Y., 2009. Chem. Rev. 109, 1948–1998.
Liu, M., Zhang, W., Chang, D., Zhang, Q., Brennan, J.D., Li, Y., 2015. Trac-Trend Anal. Chem. 74, 120–129.
Liu, J.W., Wang, Y.M., Xu, L., Duan, L.Y., Tang, H., Yu, R.Q., Jiang, J.H., 2016. Anal. Chem. 88, 8355–8358.
Loh, K.P., Bao, Q., Eda, G., Chhowalla, M., 2010. Nat. Chem. 2, 1015–1024.
Lu, C.H., Yang, H.H., Zhu, C.L., Chen, X., Chen, G.N., 2009. Angew. Chem. Int. Ed. 48, 4785–4787.
Luo, F., Zheng, L., Chen, S., Cai, Q., Lin, Z., Qiu, B., Chen, G., 2012. Chem. Commun. 48, 6387–6389.
Ma, T.Y., Tang, Y., Dai, S., Qiao, S.Z., 2014. Small 10, 2382–2389.
Mo, L.T., Li, J., Liu, Q., Qiu, L.P., Tan, W.H., 2017. Biosens. Bioelectron. 89, 201–211.
Shi, X.B., He, Y., Gao, W.L., Liu, X.Y., Ye, Z.G., Liu, H., Xiao, L.H., 2018. Anal. Chem. 90, 3661–3665.
Song, Z.P., Li, Z.H., Lin, L.H., Zhang, Y.F., Lin, T.R., Chen, L., Cai, Z., Lin, S., Guo, L.Q., Fu, F.F., Wang, X.C., 2017. Nanoscale 9, 17737–17742.
Song, Z.P., Lin, T.R., Lin, L.H., Lin, S., Fu, F.F., Wang, X.C., Guo, L.Q., 2016. Angew. Chem. Int. Ed. 55, 2773–2777.
Song, Y., Yan, X., Ostermeyer, G., Li, S.Q., Qu, L.B., Du, D., Li, Z.H., Lin, Y.H., 2018. Anal. Chem. 90, 10369–10376.

Sun, X.X., Fan, J., Fu, C.H., Yao, L.Y., Zhao, S., Wang, J., Xiao, J.X., 2017. Sci. Rep. 7, 10290.
Tan, C.L., Yu, P., Hu, Y.L., Chen, J.Z., Huang, Y., Cai, Y.Q., Luo, Z.M., Li, B., Lu, Q.B., Wang, L.H., Liu, Z., Zhang, H., 2015. J. Am. Chem. Soc. 137, 10430–10436.
Tang, Y.R., Song, H.J., Su, Y.Y., Lv, Y., 2013. Anal. Chem. 85, 11876–11884.
Tian, F., Lyu, J., Shi, J., Yang, M., 2017. Biosens. Bioelectron. 89, 123–135.
Wang, Y., Li, Z.H., Hu, D.H., Lin, C.T., Li, J.H., Lin, Y.H., 2010. J. Am. Chem. Soc. 132, 9274–9276.
Wang, Y., Li, Z.H., Weber, T.J., Hu, D.H., Lin, C.T., Li, J.H., Lin, Y.H., 2013. Anal. Chem. 85, 6775–6782.
Wang, G.B., Wang, W., Lei, J.P., Xu, P., Gao, F.L., Ju, H.L., 2013. Anal. Chem. 85, 12182–12188.
Wang, Y., Tang, L.H., Li, Z.H., Lin, Y.H., Li, J.H., 2014. Nat. Protoc. 9, 1944–1955.
Wang, C.X., Yu, P., Guo, S.Y., Mao, L.Q., Liu, H.B., Li, Y.L., 2016. Chem. Commun. 52, 5629–5632.
Wang, Y., Li, Z.H., Liu, M.S., Xu, J.J., Hu, D.H., Lin, Y.H., Li, J.H., 2017. Anal. Chim. Acta 983, 1–8.
Wu, J., Yang, S.W., Li, J.P., Yang, Y.C., Wang, G., Bu, X.M., He, P., Sun, J., Yang, J.H., Deng, Y., Ding, G.Q., Xie, X.M., 2016. Adv. Opt. Mater. 4, 2095–2101.
Xi, Q., Zhou, D.M., Kan, Y.Y., 2014. Anal. Chem. 86, 1361–1365.
Xu, S.C., Man, B.Y., Jiang, S.Z., Wang, J., Wei, J., Xu, S.D., Li, H.P., Gao, S.B., Liu, H.L., Li, Z.H., Li, H.S., Qiu, H.G., 2015. ACS Appl. Mater. Interfaces 7, 10977–10987.
Yan, F., Wang, F., Chen, Z., 2011. Sens. Actuators B: Chem. 160, 1380–1385.
Yang, G.H., Zhu, C.Z., Du, D., Zhu, J.J., Lin, Y.H., 2015. Nanoscale 7, 14217–14231.
Yuan, Y.X., Wu, S.F., Shu, F., Liu, Z.H., 2017. Chem. Commun. 50, 1095–1097.
Zhang, X.D., Xie, X., Wang, H., Zhang, J.J., Pan, B.C., Xie, Y., 2013. J. Am. Chem. Soc. 135, 18–21.
Zhang, X.L., Zheng, C., Guo, S.S., Li, J., Yang, H.H., Chen, G.N., 2014. Anal. Chem. 86, 3426–3434.
Zhang, X.D., Wang, H.X., Wang, H., Zhang, Q., Xie, J.F., Tian, Y.P., Wang, J., Xie, Y., 2014. Adv. Mater. 26, 4438–4443.
Zhang, Y., Zheng, B., Zhu, C.F., Zhang, X., Tan, C.L., Li, H., Chen, B., Yang, J., Chen, J.Z., Huang, Y., Wang, L.H., 2015. Adv. Mater. 27, 935–939.
Zhu, C.F., Zeng, Z.Y., Li, H., Li, F., Fan, C.H., Zhang, H., 2013. J. Am. Chem. Soc. 135, 5998–6001.
Zhu, C., Du, D., Lin, Y., 2015. 2D Mater. 2, 032004.